Supporting Information

Iron transport in cancer cell culture suspensions measured by cell magnetophoresis

Xiaoxia Jin,[†‡] Jeffrey J. Chalmers,[‡] Maciej Zborowski[†]*

[†]Department of Biomedical Engineering/ND20
Lerner Research Institute
Cleveland Clinic
9500 Euclid Avenue
Cleveland, OH 44195

[‡]William G. Lowrie Department of Chemical and Biomolecular Engineering
The Ohio State University
140 W 19th Avenue
Columbus, OH 43210

*Corresponding Author: zborowm@ccf.org, tel. 216-445-9330, Fax: 216-444-9198

Table of Contents

Magnetic susceptibility of culture media

A standard, complete liquid cell culture media was used for maintaining all eight cancer cell lines in culture (Table 1 in main text). More than 95% volume of the complete cell media is diamagnetic water. Magnetic susceptibilities of the liquid media components are listed in Table S1. Most of them are not less diamagnetic as water except paramagnetic ferric nitrate. Ferric nitrate is a part of DMEM liquid media at a low concentration, 0.10 mg/L; consequently its contribution to the bulk magnetic susceptibility of DMEM media was negligible, as shown here by comparing weighed susceptibility contributions (a product of volume fraction, ϕ, and the volume magnetic susceptibility, χ) of the ferric nitrate and water components to the total media magnetic susceptibility: for ferric nitrate $\phi\chi(Fe(NO_3)_3) = 0.10$ mg/L/$(1.68 \times 10^6$ mg/L$) \times 796.15 \times 10^{-6} = 4.7 \times 10^{-11}$, where 1.68×10^6 mg/L is the mass density of ferric nitrate; and for water $\phi\chi\,(H_2O) \approx 0.95 \times (-9.04 \times 10^{-6}) = -8.59 \times 10^{-6}$. (The bulk volume magnetic susceptibility of the media is the weighted sum of the susceptibilities of its components.) Thus, the water contribution to the DMEM magnetic susceptibility is approximately five orders of magnitude greater than that of the ferric nitrate.

Another source of paramagnetic iron is fetal bovine serum (FBS) used to supplement DMEM in application to cell culture, typically at 10% (w/v). Kakuta et al. [1] reported an average value of 2.40 mg/L iron in FBS by measuring 13 lots of commercial FBS. Assume conservatively that all these iron atoms are in high spin state with a magnetic susceptibility of $14{,}000 \times 10^{-9}$ L/mol (same as that in metHb RBC [2, 3]). It follows that the weighed FBS Fe magnetic susceptibility contribution in the media is $\phi\chi$

(FBS Fe) $= 0.1 \times 2.4 \times 10^{-3}/56 \times 4\pi \times 14{,}000 \times 10^{-9} = 7.5 \times 10^{-10}$, which also can be ignored in comparison with the contribution of water calculated above, $\phi\chi$ (H_2O) ≈ -8.59×10^{-6}.

For CTV analysis, cells were washed once with and resuspended in PBS containing 0.1% Pluronic F-68. The composition of the buffer was different from that commonly used for magnetic cell separation, i.e. PBS with 0.5% BSA and 2 mM EDTA. The replacement of BSA and EDTA by Pluronic was motivated by the following reasons. The role of EDTA in the buffer used for cell separation is to bind free divalent ions (Ca^{2+}, Mg^{2+}) in order to minimize cell adhesion to surfaces and to each other and thus avoid undesirable, non-specific cell losses and cell-cell aggregation. The BSA saturates potential cell binding sites in the fluid pathway and also helps preventing cell losses to non-specific cell adhesion. By the same token, however, EDTA forms strong complexes with Fe (III) and therefore could interfere with the CTV magnetophoretic measurements by driving the iron transport out of the cell. Moreover, BSA contains iron related to its production process which may further interfere with the CTV results. On the other hand, protective effect of Pluronic in cell cultures has been reported by others by preventing loss of cell viability in a gas sparged or bubble-free environments [2]. During our experiments, no cell aggregation or loss of viability was observed by using buffer PBS + 0.1% Pluronic. The iron concentration in PBS + 0.1% Pluronic buffer was comparable to that of the original PBS solution but lower than that of the PBS + 2 mM EDTA + 0.5% BSA buffer, as expected (Table S2). Importantly, the iron concentration in all three buffers measured by ICP-MS and listed in Table S2 was much lower than the

intracellular iron concentration measured in the cancer cell lines used in this study (compare Table S2 with Table 2).

Characterization of cancer cells

Cells cultured in the complete media were collected at subconfluence, washed, and suspended in PBS. Cell size distributions were determined by Coulter counter. The mean cell diameters for all eight cancer cell lines are included in Table 2 (main text). Two paramagnetic metal concentrations in the cells, Fe and Mn were measured by ICP-MS and recalculated to the intracellular content using the measured mean cell diameter (Table 2). It is noteworthy that two hepatocellular cell lines, Hep 3B and Hep G2, possess the highest Fe and Mn content. This is consistent with the metabolic function of the liver and its role as the iron storage site in the body. It is well known that a number of diseases of the liver, such as liver fibrosis, cirrhosis, and hepatoma are related to the accumulation of iron in the hepatocyte [3].

In order to control for the possible effect of cell viability on its magnetophoretic mobility, we have measured the cell viability and mobility over time in culture without replacement of new media (no cell passaging), for up to eight days. The representative time course for HeLa cell line is shown in Figure S1. As expected, the cell viability started to decrease after day 3 in culture, accompanied by a concomitant cell growth inhibition after day 4 in culture. There was no statistically significant change in the cell mean magnetophoretic mobility (MM), however. The mean MM of HeLa cells stayed slightly positive, which is different from the slightly negative mean MM of the oxygenated RBC used as one of the reference standards (Figure S3A). These results

suggest that the population mean cell MM is insensitive to the population mean cell viability in the range tested, and therefore any observed differences in the cell mean MM are related to factors other than the cell viability. This is illustrated for the case of the soluble iron addition to culture (as described in the main text) resulting in a significant increase in the cell mean MM over the unmodified media that was also insensitive to the drop of the cell viability over time (Figure S2). Representative examples of the U-937 and HeLa cell MM histograms resulting from the CTV analysis are shown in Figure 1. The cumulative MM histograms, also shown in Figure 1, were used to estimate the high-mobility "magnetic" cell subpopulation (as described in the main text).

Cell magnetophoretic mobility analysis by CTV

Magnetophoretic mobility (MM, or *m* for short) is defined as a ratio of the field-induced velocity, u_m, and the magnetic force field, S_m:

$$m = \frac{u_m}{S_m} \tag{1}$$

The magnetic force field is a product of the magnetic field *H* and the gradient of the magnetic field *B*:

$$S_m = \frac{1}{2} H \frac{dB}{dx} \tag{2}$$

where H is the magnetic field strength (in A/m) and B is the magnetic field intensity (in tesla, T). The expression in Equation 2 applies to the magnetic field gradient in one dimension (along x-axis), applicable to the CTV design. For paramagnetic and diamagnetic contributions in a living cell the formula for the magnetophoretic mobility m simplifies considerably to an expression that depends only on the cell and the fluid properties (but not the magnetic field):

$$m = \frac{V}{6\pi\eta R}\Delta\chi \tag{3}$$

Thus, the measurement of cell magnetophoretic mobility (Equation 1) can be used to measure the cell volume magnetic susceptibility (Equation 3) and, providing that additional details about the cell physical properties and elemental composition are known, the intracellular concentration of paramagnetic species. This is illustrated here on the example of RBC, used as a reference standard. The RBC hydrodynamic radius, R = 3.85 μm; its volume, V = 88.4 μm^3; the aqueous solution viscosity at 20 C is $\eta = 0.96\times10^{-3}$ kg/m-s. The red blood cell magnetic susceptibility relative to that of the solution, $\Delta\chi$:

$$\Delta\chi = \chi_{RBC} - \chi_{H2O} \tag{4}$$

where $\chi_{H2O} = -9.04\times10^{-6}$ is the magnetic volume susceptibility of water.[4] The red blood cell volumetric magnetic susceptibility is the weighted sum of the volume susceptibilities of its components, that is water, deoxyhemoglobin and the protein (globin)

part of the hemoglobin molecule and it depends on the oxygen saturation of oxyhemoglobin.[5] The methemoglobin contribution to the erythrocyte magnetic susceptibility has a similar form, for known volume fraction and magnetic susceptibility of methemoglobin.[6, 7] In the final analysis, one calculates for oxygenated RBC: $\Delta\chi = -0.185\times10^{-6}$ and for methemoglobin RBC, 4.61×10^{-6}. The resulting MMs of the RBC (calculated by inserting $\Delta\chi$ into Equation 3) for oxyHb RBC, m = -0.226×10^{-6} mm^3/T.A.s and metHb RBC, m = 4.61×10^{-6} mm^3/T.A.s agree well with the experimentally measured mean MM RBC values by the CTV, oxyHb RBC m = $(-0.25 \pm 1.23)\times10^{-6}$ mm^3/T.A.s and metHb RBC m = $(4.7 \pm 1.5)\times10^{-6}$ mm^3/T.A.s (Figure S3). The type of MM analysis described here for the RBC standards was repeated for cancer cell lines selected for this study and the results interpreted in terms of the intracellular, high-spin iron and manganese paramagnetic contributions to the cell magnetic susceptibility.

The cell motion in the strong magnetic energy density gradient (described in the main text) is recorded using a microscope (Olympus BXFM-F, Tokyo, Japan) with attached 12-bit monochrome video camera (Retiga Exi, QImaging, Burnaby, BC, Canada). The image size is 640 x 480 pixels with 1 x 1 binning. The digital images are acquired to PC RAM using software (Video Savant, IO Industries, London, Ontario, Canada) and saved to the PC hard drive. The CTV algorithm uses five consecutive frames to establish the most probable paths of cells (N = 700 to 2,000 cells per sample) and reports 2D locations.[8] With the aid of EXCEL (Microsoft Corp., Redmond, WA) spreadsheet macros, a linear fit of location-time data gives the velocity components of each particle.

Magnetic cell separation

Following magnetic separation (Figure S4, as described in the main text) the "magnetic" and "non-magnetic" fractions were re-cultivated in the same complete media as the original cell sample. After approximately 72 hrs incubation, cells were harvested and analyzed by CTV and ICP-MS and the results compared to the starting populations (columns "B" and "A" in Tables S3 and S4, respectively). For the "magnetic" HeLa cell fraction, the cell mean MM was reduced from 5.51×10^{-5} to 1.38×10^{-5} mm^3/TAs , and Fe content decreased from 430 to 160 fg/cell (Figure S5). No significant changes were found in the "non-magnetic" cell subpopulation (Table S3). Similarly for the K-562 cell line: before re-culture, the "magnetic" cell mean MM was 5.36×10^{-5} mm^3/TAs and the mean intracellular iron content was 330 fg Fe/cell, which dropped to 1.60×10^{-5} mm^3/TAs and 103 fg Fe/cell, respectively (Table S4, columns "B"). Again, no significant changes were found in the "non-magnetic" cell subpopulation.

Compared to the intracellular Fe content, the Mn cell content was much lower (Tables 1, S3, S4 and Figure S5) and therefore its contribution to the cell magnetic susceptibility and magnetophoretic mobility was considered negligible. For instance for HeLa cells, if all forms of the intracellular iron (46 fg/cell) are in the form of high-spin FeO with the magnetic susceptibility [9] of $7{,}180 \times 10^{-6}$, and all forms of manganese (1.7 fg/cell) are in the form of MnO with a magnetic susceptibility of $4{,}680 \times 10^{-6}$, the contributions of FeO and MnO to the bulk cell magnetic susceptibility are 3.58×10^{-8} and 9.34×10^{-10}, respectively, indicating that MnO contribution is approximately 40 times lower than that of FeO.

Intracellular ferritin by TEM and TfR1 (CD71) expression and cell cycle analysis by flow cytometry

The effect of exogenous soluble iron in the form of FAC or $Fe(NO_3)_3$ on the cell biology was tested by measuring levels of surface transferrin receptors (TfR1) in both K-562 and HeLa cells. The TfR1 receptor levels were measured by immunofluorescence labeling with PE-conjugated monoclonal anti-human TfR1 (CD71) monoclonal antibody. The cell suspension collected from T-flask was washed by a degassed labeling buffer containing 1× PBS, 2 mM EDTA, and 0.5% BSA. Thirty μL/10^6 cells of primary antibody, anti-human CD71-PE (BD Pharmingen) was then added to the cell pellet. After 30 minutes of incubation on ice, cells were washed once with the labelling buffer and resuspended in 0.4 mL PBS for flow cytometry analysis. Control sample consisted of unstained cell suspension (negative control). Stained cell samples that were not analyzed immediately after labeling were fixed using a 1% v/v formaldehyde (Polysciences, Inc. Warrington, PA) in PBS solution for later analysis. The cells were kept in dark at 4°C after fixing till analysis on the flow cytometer. The cell fluorescence analyses were performed in the LRI Flow Cytometry Core (FACS, BD LSR I, BD Biosciences, San Jose, CA, using a FACSDiva software V5.2.0). QuantiBRITE™ PE fluorescent beads (BD Pharmingen) were used to estimate the number of antibodies (anti-CD71-PE) bound per cell. At least 10,000 cells were evaluated for each sample and the analysis of the flow cytometry data was conducted using a freeware provided by Joe Trotter of the Scripps Institute, La Jolla, CA (WinMDI).The surface TfR1 was quantitatively measured using QuantiBRITE™ PE beads and normalized to the TfR1 number expressed on control cells at 0 hr (control cells were incubated in the complete media without iron addition). The

time course of the TfR1 expression shows pronounced decrease in the transferrin receptor expression, followed by return (HeLa) or an over-shoot (K-562) of the expression with respect to the initial levels (Figure S6). The observed difference between TfR1 expression levels over time in HeLa and K-562 cells was compatible with the longer lag period expected of the adherent (HeLa) than suspension (K-562) cell culture. Thus, it took only about 1 hr incubation for the surface TfR1 signal in K-562 cell to reach a minimum before starting to rise but a longer time of about 5 hrs for HeLa cell before starting to return to the control TfR1 signal level. After about 24 hrs incubation, surface TfR1s expression reached the level of control cells for HeLa cells or increased above the control level for K-562 cells. The data show that K-562 cells expressed more TfR1s than HeLa cells after reaching a maximum. After about 48 hrs through the end of the experiment at 72 hr, the level of surface TfR1 started to decline again (Figure S6).

In an effort to better characterize the "magnetic" fraction obtained by label-free magnetic separation of the HeLa cells, the aliquots of the original sample and the magnetic fraction were subjected to cell cycle analysis by flow cytometry. Iron plays an important role in the DNA synthesis. Consistent with the assumption of an increased demand for intracellular iron in actively dividing cells, we were interested in looking for evidence of a higher number of actively dividing cells in the "magnetic" fraction as compared to the original sample. Thus, cells in G0/G1 phase that may have lower demand for intracellular iron than cells in the S and M phases were expected to be separated in the "non-magnetic" fraction. The cellular DNA content in HeLa cells was measured before and after MACS separation (as described in the main text). The cellular DNA content was measured by fluorescent stain binding and flow cytometry. As

propidium iodide (PI) binds stoichiometrically to the double-stranded DNA, the fluorescent intensity of a stained cell offers a direct measure of the DNA content in that cell. The cells were first permeabilized by fixation with 70% ethanol at 4 °C for 30 min. Cell suspension was then centrifuged at about 200 g for 6 minutes and resuspended in PBS with a concentration of 1×10^6 cells/mL. Following addition of 5 µL RNase (DNase-free) to 1 mL of cell suspension, the cell mixture was incubated at 37 °C for 30 minutes, chilled on ice and 100 µL propidium iodide was added (PI, Roche Applied Science, Indianapolis, IN). The red cell fluorescence (indicating PI binding) was measured by flow cytometry and analyzed using ModFit LT™ software package (Verity Software House, Topsham, ME). Cells in G0 or G1 phases possess a normal diploid DNA content, which are represented by the narrow peak on the left side of the DNA histogram (Figure S8). Cells in G2 or M phases contain twice the normal DNA content, and are represented by the second, smaller peak located on the right side of the distribution with twice the cell fluorescence intensity value. As the DNA is synthesized during S phase, the resulting cell fluorescence intensity is distributed continuously between G0/G1 and G2/M phases (Figure S8). The HeLa cell cycle distribution was shifted slightly towards the actively dividing cells (S, G2 and M phases) in the "magnetic" fraction as compared to the original sample (before separation) and the "non-magnetic" fraction without reaching statistical significance (Table S5).

Table S-1 Volume magnetic susceptibilities of complete cell culture liquid media components (listed in Table 1)

Substance	Temperature (K)	$\chi \times 10^6$ (SI)*	Concentration in normal media (g/L)
H_2O	293	-9.04	~985
$CaCl_2$	ord.	-13.32	0 - 0.2
$Ca(NO_3)_2$	ord.	-8.80	0 - 0.1
$MgSO_4$	294	-13.88	0.04884 - 0.09767
KCl	ord.	-13.04	0.33 - 0.40
KNO_3	ord.	-8.83	0 - 0.000076
NaCl	ord.	-14.11	4.505 - 6.800
Alanine	-	-10.11	0 - 0.025
Asparagine	288	-10.20	0 - 0.05682
Aspartic acid	285	-10.05	0 - 0.03
Glutamic acid	-	-9.78	0 - 0.075
Glycine	323	-10.63	0.0075 - 0.0500
Isoleucine	-	-9.47	0.050 - 0.105
Leucine	-	-10.51	0.050 - 0.105
Tryptophan	-	-10.88	0.005 - 0.016
Tyrosine	-	-10.63	0.02883 - 0.10400
Valine	-	-9.80	0.020 - 0.094
vitamin B-12	-	-8.67	0 - 0.000136
D-glucose	298	-10.92	1.0 - 4.5
$Fe(NO_3)_3 \cdot 9H_2O$	293	796.15	0 - 0.0001

*Volume magnetic susceptibilities, χ, in SI unit system, χ(SI), were calculated from mass, χ_g, or molar, χ_m, magnetic susceptibilities in CGS units, χ(CGS), and mass densities, ρ, and molecular weights, Mw, of the respective components as provided by CRC Handbook of Chemistry and Physics [9] using the following equations:

χ (CGS) = $\rho\chi_g$ (CGS), χ (CGS) = $\rho\chi_m$ (CGS)/Mw, and χ (SI) = $4\pi\chi$ (CGS)

Table S-2 Fe and Mn content in suspending media analyzed by ICP-MS

	Fe (ng/mL)	Mn (ng/mL)
PBS (1×)	2.3	< 0.5
0.1% Pluronic + PBS	2.5	< 0.5
PBS + 2 mM EDTA + 0.5% BSA	8	< 0.5

Table S-3 MACS separation results on HeLa cell

	Cell # ($\times 10^6$)	Viability (%)	Mean *m* (mm^3/TAs)		Fe (fg/cell)		Mn (fg/cell)	
			A	B	A	B	A	B
Before separation	42.4	91.9	3.33×10^{-6}	-	46	-	1.7	-
Negative fraction	36.7	91.7	-6.92×10^{-7}	-1.56×10^{-8}	38	38	1.7	1.1
Positive fraction	0.46	81.7	5.51×10^{-5}	1.38×10^{-5}	430	160	4.3	4.5
metHb RBC	-	-	4.74×10^{-6}		100		< 0.04	

A - Data were obtained directly after separation. B - Following magnetic separation, both positive and negative fractions were inoculated into T flasks containing fresh media (as shown in Table S1) and re-cultured for approximately 72 hours. Growth rates and the cell number concentrations were comparable for both cell fractions at the end of the re-culture period. The cells were subsequently re-analyzed by CTV and ICP-MS

Table S-4 MACS separation results on K-562 cell

	Cell # ($\times 10^6$)	Viability (%)	Mean *m* (mm^3/TAs)		Fe (fg/cell)		Mn (fg/cell)	
			A	B	A	B	A	B
Before separation	26.6	91.2	3.37×10^{-6}	-	48	-	0.9	-
Negative fraction	26.5	89.4	-1.26×10^{-6}	-7.78×10^{-8}	40	44	0.7	0.5
Positive fraction	0.26	75.3	5.36×10^{-5}	1.60×10^{-5}	330	103	3.5	2.6

A - data was obtained directly after separation. B - Following magnetic separation, both positive and negative fractions were inoculated into T flasks containing fresh media (as shown in Table S1) and re-cultured for approximately 72 hours. Growth rates and the cell number concentrations were comparable for both cell fractions at the end of the re-culture period. The cells were subsequently re-analyzed by CTV and ICP-MS

Table S-5 Percentage of cells in each phase of the cell cycle for HeLa cells before and after separation.

	G0/G1 (%)	S (%)	G2/M (%)
Before separation	82.56	13.63	3.80
Negative fraction	83.06	13.50	3.44
Positive fraction	80.69	14.71	4.60

References

(1) Kakuta, K.; Orino, K.; Yamamoto, S.; Watanabe, K. *Comp Biochem Physiol A Physiol* **1997**, *118*, 165-169.

(2) Tharmalingam, T.; Ghebeh, H.; Wuerz, T.; Butler, M. *Mol Biotechnol* **2008**, *39*, 167-177.

(3) Bonkovsky, H. L. *Am J Med Sci* **1991**, *301*, 32-43.

(4) Weast, R. C. *CRC Handbook of Chemistry and Physics*, 67 ed.; CRC Press, Inc.: Boca Raton, FL, 1986.

(5) Spees, W. M.; Yablonskiy, D. A.; Oswood, M. C.; Ackerman, J. J. *Magn Reson Med* **2001**, *45*, 533-542.

(6) Coryell, C.; Stitt, F.; Pauling, L. *J Am Chem Soc* **1937**, *59*, 633-642.

(7) Graham, M. D. *Journal de Physique, Colloque C.1* **1984**, *45 (Suppl.)*, C1/779-C771/784.

(8) Nakamura, M.; Zborowski, M.; Lasky, L. C.; Margel, S.; Chalmers, J. J. *Exp Fluids* **2001**, *30*, 371-380.

(9) Weast, R. C., Ed. *CRC Handbook of Chemistry and Physics*, 62nd ed.; CRC Press, Inc.: Boca Raton, Fla., 1981.

(10) Richardson, D. R.; Kalinowski, D. S.; Lau, S.; Jansson, P. J.; Lovejoy, D. B. *Biochim Biophys Acta* **2009**, *1790*, 702-717.

Legends for Figures

Figure S-1 HeLa cell growth curve (blue diamonds), viability curve (red triangles), and MM curve (black circles) in complete media (without passaging). Error bar represents one standard deviation.

Figure S-2 Comparison of MM (*m*, circles) and viability (triangles) of HeLa cells incubated in complete media (dark gray) and media with 0.5 mg/mL $Fe(NO_3)_3$ addition (black) without passaging. Error bar represents one standard deviation.

Figure S-3 Magnetophoretic mobility (MM, *m*) histograms of oxygenated (A) and methemoglobin (B) containing RBCs, by CTV. The second axis at the bottom shows the corresponding magnetic field-induced velocity (u_m) values.

Figure S-4 MM histograms of HeLa cell before and after separation. Note change in scale of horizontal axis and presence of highly magnetic cells in the "positive fraction".

Figure S-5. Comparison of cell MM and paramagnetic metal content before and after magnetic separation, and following additional time in culture. A. Data were obtained directly after separation. B. Data were obtained after re-culture for approximately 72 hrs.

Figure S-6 Surface TfR1 expression on K-562 (circles) and HeLa (triangles) cells incubated in media supplemented with FAC (solid symbols) or $Fe(NO_3)_3$ (open symbols) relative to the TfR1 expression on control K-562 or HeLa cells (incubated in the complete media without iron addition).

Figure S-7 Representative TEM images of HeLa cells (A) incubated in media supplemented with $Fe(NO_3)_3$ and (B) without soluble iron supplementation. Ferritin iron cores could be easily identified in (A) but not in (B).

Figure S-8 Cell cycle analysis on HeLa feed sample (prior to magnetic separation) by flow cytometry and ModFit™ software package. The DNA profiles for the positive and negative fractions after separation were very similar to the one shown here and therefore are not included. The legend shows color key for different cell cycle phases and artifacts (debris and apoptotic cells) fitted to the DNA profile by the program.

Figure S-9 Schematic illustration of the dual role of high intracellular iron concentration on A) suppression of TfR1 expression and B) activation of ferritin synthesis (adapted from Richardson DR et al. [10]). Here IRP1 and IRP2 denote iron regulatory proteins 1 and 2, respectively.

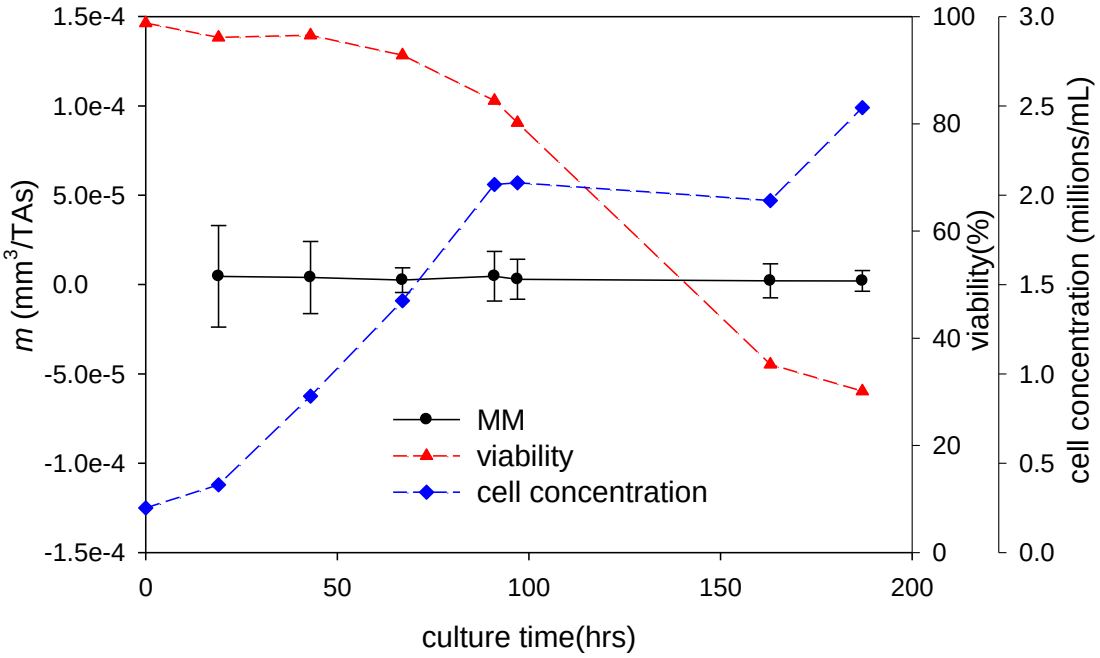

Figure S-1 HeLa cell growth curve (blue diamonds), viability curve (red triangles), and MM curve (black circles) in complete media (without passaging). Error bar represents one standard deviation.

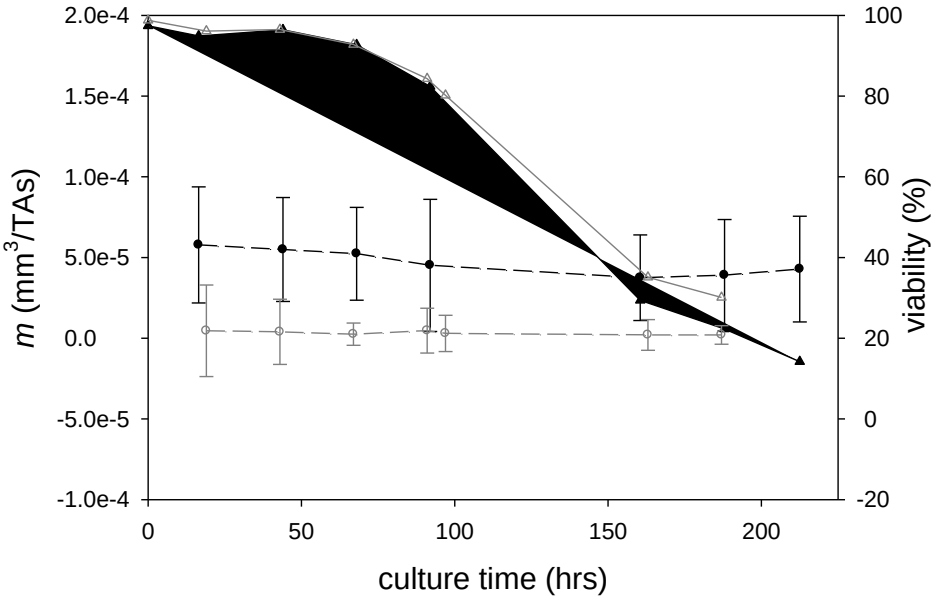

Figure S-2 Comparison of MM (*m*, circles) and viability (triangles) of HeLa cells incubated in complete media (dark gray) and media with 0.5 mg/mL $Fe(NO_3)_3$ addition (black) without passaging. Error bar represents one standard deviation.

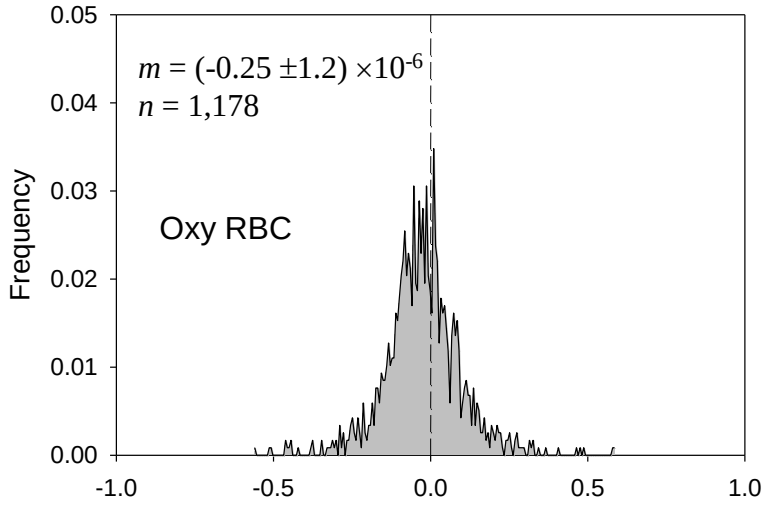

(A)

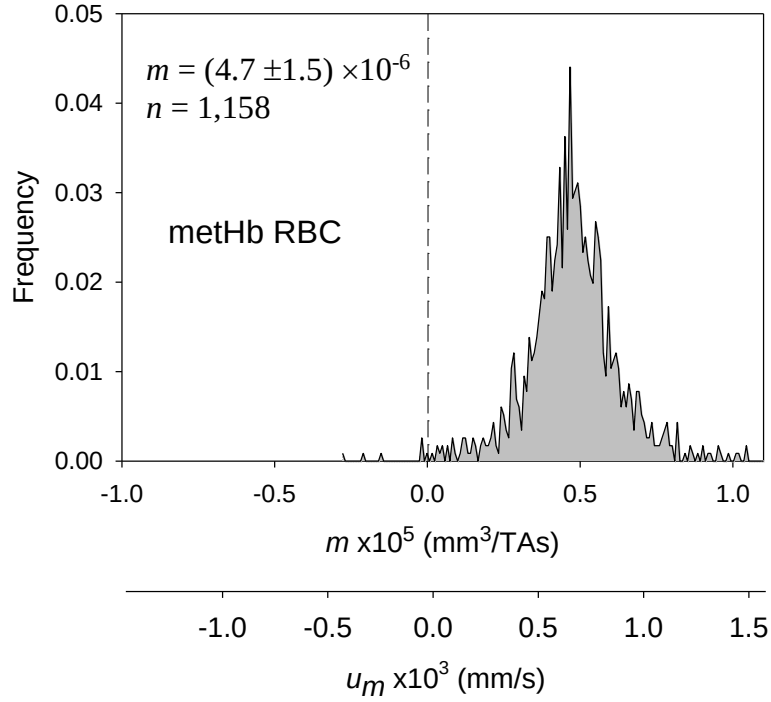

(B)

Figure S-3 Magnetophoretic mobility (MM, *m*) histograms of oxygenated (A) and methemoglobin (B) containing RBCs, by CTV. The second axis at the bottom shows the corresponding magnetic field-induced velocity (u_m) values.

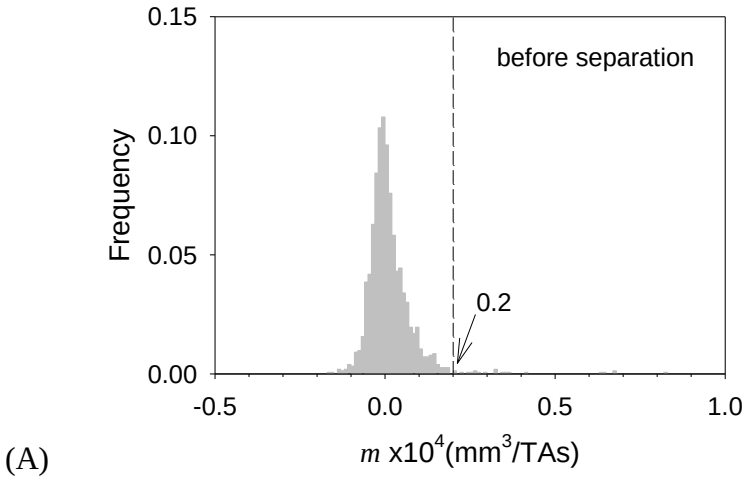

(A)

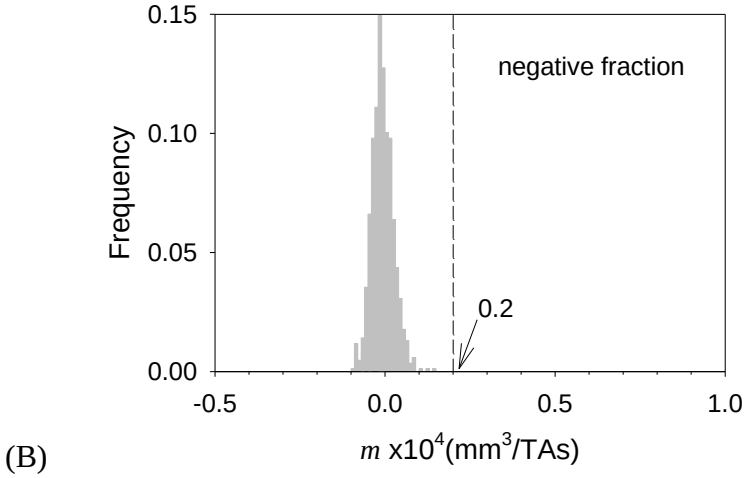

(B)

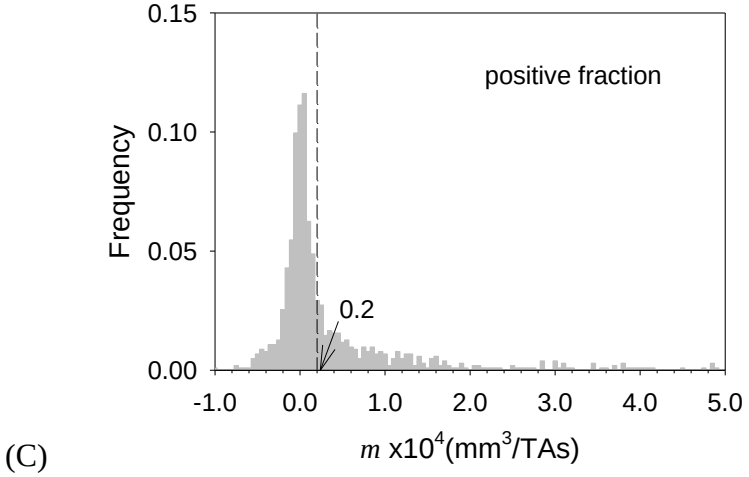

(C)

Figure S-4 MM histograms of HeLa cell before and after separation. Note change in scale of horizontal axis and presence of highly magnetic cells in the "positive fraction".

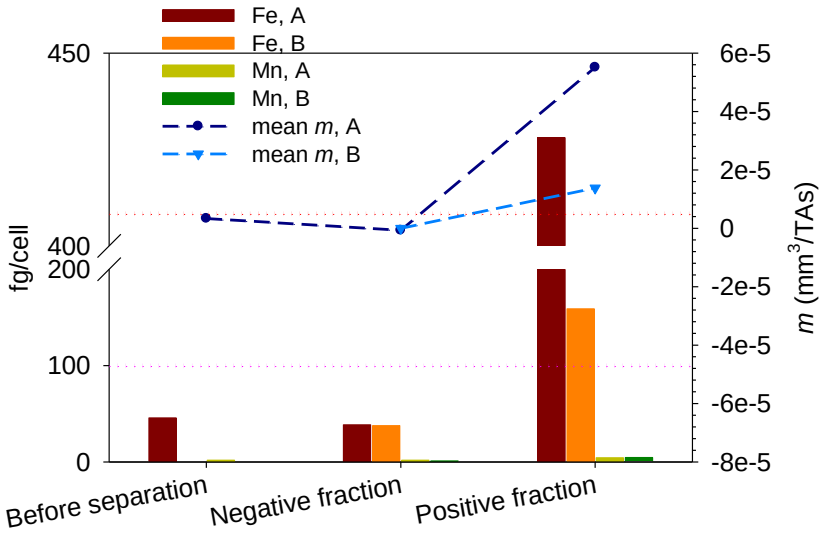

Figure S-5 Comparison of cell MM and paramagnetic metal content before and after magnetic separation, and following additional time in culture. A. Data were obtained directly after separation. B. Data were obtained after re-culture for approximately 72 hrs.

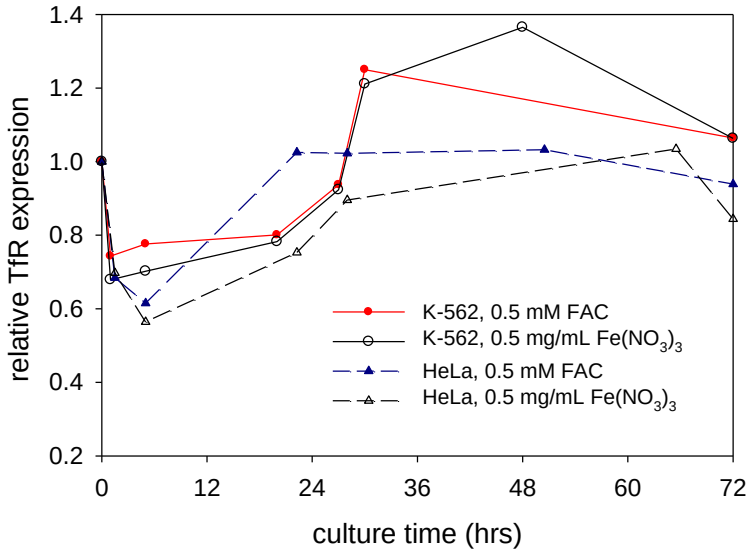

Figure S-6 Surface TfR1 expression on K-562 (circles) and HeLa (triangles) cells incubated in media supplemented with FAC (solid symbols) or $Fe(NO_3)_3$ (open symbols) relative to the TfR1 expression on control K-562 or HeLa cells (incubated in the complete media without iron addition).

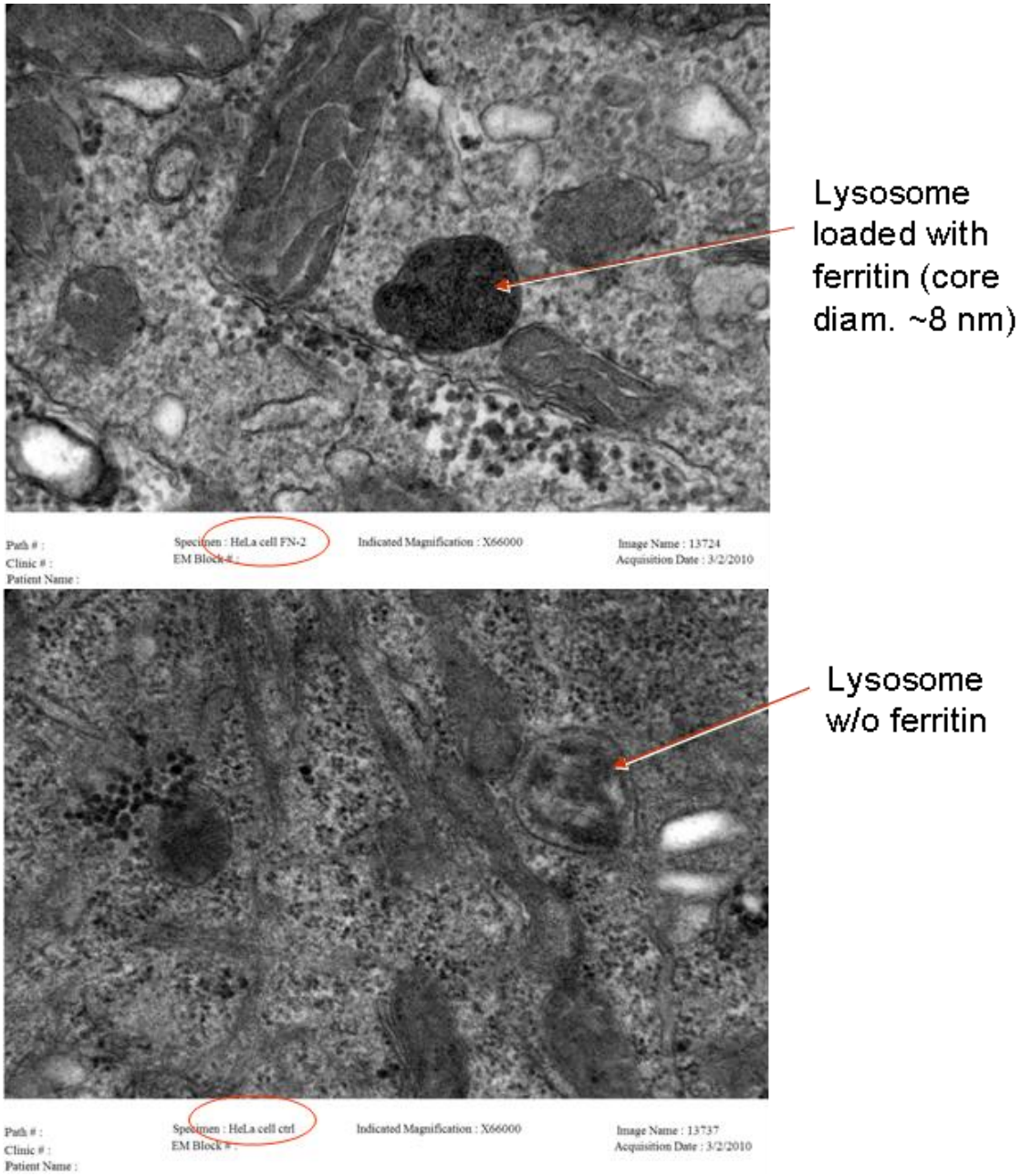

Figure S-7 Representative TEM images of HeLa cells (A) incubated in media supplemented with $Fe(NO_3)_3$ and (B) without soluble iron supplementation. Ferritin iron cores could be easily identified in (A) but not in (B).

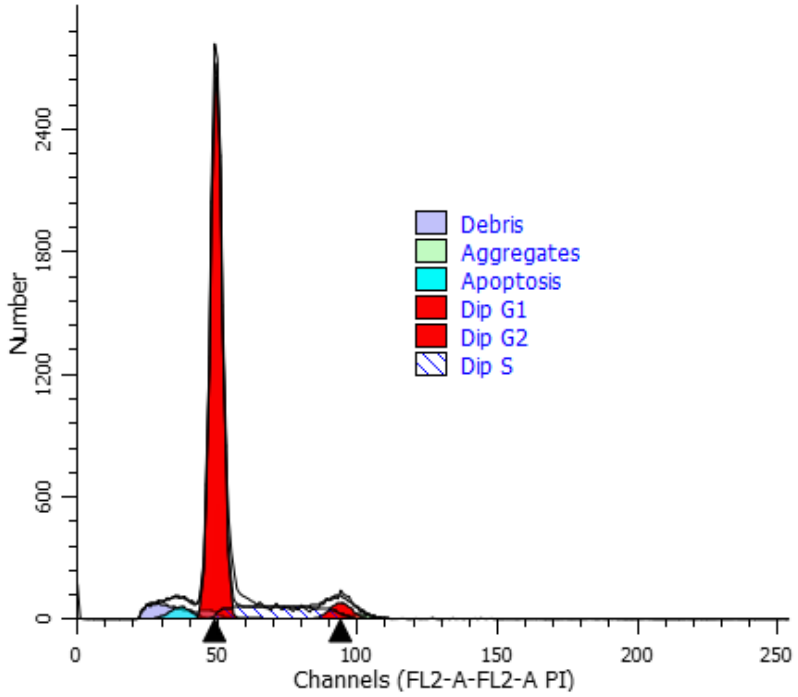

Figure S-8 Cell cycle analysis on HeLa feed sample (prior to magnetic separation) by flow cytometry and ModFit™ software package. The DNA profiles for the positive and negative fractions after separation were very similar to the one shown here and therefore are not included. The legend shows color key for different cell cycle phases and artifacts (debris and apoptotic cells) fitted to the DNA profile by the program.

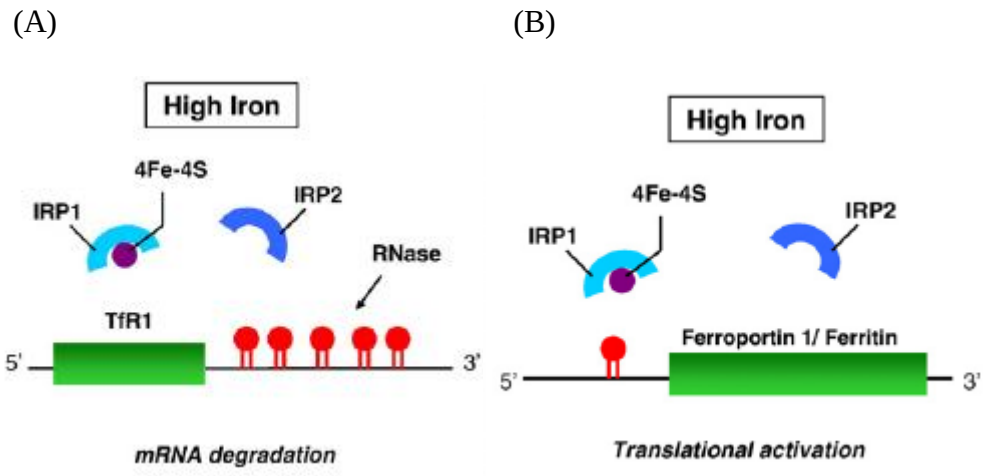

Figure S-9 Schematic illustration of the dual role of high intracellular iron concentration on A) suppression of TfR1 expression and B) activation of ferritin synthesis (adapted from Richardson DR et al. [10]). Here IRP1 and IRP2 denote iron regulatory proteins 1 and 2, respectively.